Long α helices projecting from the membrane as the dimer interface in the voltage-gated H^+ channel

Yuichiro Fujiwara,[1] Tatsuki Kurokawa,[1] Yasushi Okamura[1,2]

[1]Integrative Physiology, Graduate School of Medicine, and [2]Graduate School of Frontier Biosciences, Osaka University, Osaka 565-0871, Japan

The voltage-gated H^+ channel (Hv) is a H^+-permeable voltage-sensor domain (VSD) protein that consists of four transmembrane segments (S1–S4). Hv assembles as a dimeric channel and two transmembrane channel domains function cooperatively, which is mediated by the coiled-coil assembly domain in the cytoplasmic C terminus. However, the structural basis of the interdomain interactions remains unknown. Here, we provide a picture of the dimer configuration based on the analyses of interactions among two VSDs and a coiled-coil domain. Systematic mutations of the linker region between S4 of VSD and the coiled-coil showed that the channel gating was altered in the helical periodicity with the linker length, suggesting that two domains are linked by helices. Cross-linking analyses revealed that the two S4 helices were situated closely in the dimeric channel. The interaction interface between the two S4 and the assembly interface of the coiled-coil domain were aligned in the same direction based on the phase angle calculation along α helices. Collectively, we propose that continuous helices stretching from the transmembrane to the cytoplasmic region in the dimeric interface regulate the channel activation in the Hv dimer.

INTRODUCTION

Voltage-gated ion channels play fundamental roles in electronic signals in many organs such as brain and heart (Armstrong and Hille, 1998; Jan and Jan, 2012). The voltage-gated H^+ channel (Hv) evokes H^+ conductance essential for the production of reactive oxygens in phagocyte (Decoursey, 2003; Okochi et al., 2009; Ramsey et al., 2009; El Chemaly et al., 2010), for triggering of sperm locomotion (Lishko et al., 2010), and for conditioning the global climate by algae (Taylor et al., 2012).

The classical voltage-gated ion channels (voltage-gated Na^+, K^+, and Ca^{2+} channels: Nav, Kv, and Cav) are tetramers (Kv) or pseudotetramers (Nav and Cav) (Bezanilla, 2000), forming an ion permeation pathway in the center. Four voltage-sensor domains (VSDs) operate independently of each other on the periphery (Long et al., 2005; Payandeh et al., 2011). In contrast, in Hv, VSD is responsible for both voltage sensing and proton permeation (Ramsey et al., 2006; Sasaki et al., 2006). Hv assembles as a dimeric channel (Koch et al., 2008; Lee et al., 2008; Tombola et al., 2008), and the coiled-coil domain in the cytoplasmic C terminus underpins the dimerization (Fujiwara et al., 2012). Thus, Hv has a unique and simple design: two VSDs and a coiled-coil.

In the dimeric Hv, each channel protomer cooperates with one another during gating, providing a twofold stronger voltage dependence with a slow activation (Gonzalez et al., 2010; Musset et al., 2010; Tombola et al., 2010), which elicits physiological significance in phagosomes. Mutations in the transmembrane VSDs alter characteristics of the cooperative gating (Musset et al., 2010; Tombola et al., 2010; Qiu et al., 2013). A certain level of physical intersubunit contact between the two VSDs at the extracellular end of S1 has been shown by biochemical approaches (Lee et al., 2008), suggesting that two S1 helices in the transmembrane VSDs interact with each other. In addition, mutations in the coiled-coil domain can alter the gating properties (Fujiwara et al., 2012), demonstrating that the cytoplasmic coiled-coil domain downstream of S4 interacts functionally with the transmembrane VSD and mediates the cooperative gating. Thus, various views of interdomain interaction have been proposed. In the amino acid sequence, the coiled-coil domain is located just downstream of S4, and a direct connection between S4 and the coiled-coil domain is assumed to serve as an intermediary of the functional interaction, as we proposed previously (Fujiwara et al., 2012). However, details of the structure connecting the two domains remain unknown. In addition, the positional relationship between two S4 helices tied by the coiled-coil has not been examined and might be one of the key factors for the channel gating. Thus, structural bases of assembly and gating need to be further explored. In this

Correspondence to Yuichiro Fujiwara: fujiwara@phys2.med.osaka-u.ac.jp; or Yasushi Okamura: yokamura@phys2.med.osaka-u.ac.jp

T. Kurokawa's present address is Dept. of Synthetic Chemistry and Biological Chemistry, Graduate School of Engineering, Kyoto University, Kyoto 606-8501, Japan.

Abbreviations used in this paper: A.A., amino acids; DDM, dodecyl maltoside; Hv, voltage-gated H^+ channel; VSD, voltage-sensor domain.

The Rockefeller University Press $30.00
J. Gen. Physiol. Vol. 143 No. 3 377–386
www.jgp.org/cgi/doi/10.1085/jgp.201311082

study, we therefore aimed to understand the interdomain interactions: the cytoplasmic coiled-coil to transmembrane VSD interactions (Figs. 1 and 2) and the transmembrane VSD to VSD interactions (Figs. 3 and 4) in the dimeric Hv. In both cases of the interactions, the periodicity of α helix was observed. Based on this helical periodicity, we constructed a model of the helix orientation and connection in the Hv dimer, where two S4 helices of VSDs were close to each other in the dimeric interface and twisted in a coiled-coil structure in the cytoplasmic region, forming the long helices that stretch from the transmembrane to the cytoplasmic region.

MATERIALS AND METHODS

Molecular cloning and construction

We used a mouse Hv clone (mHv1/VSOP) (Sasaki et al., 2006) for all experiments in this study. The cDNAs for WT and mutant mHv1/VSOP channels were subcloned into the pIRES-EGFP expression vector (Takara Bio Inc.). Mutant mHv1/VSOP clones, with point mutations, deletion and insertion, were made by site-directed mutagenesis or circular PCR ligation protocols with appropriate mutant primers. A series of linker mutant channels was constructed, where the coiled-coil domain was shifted upstream (reduction of the linker length; −1 to −10 amino acids [A.A.]) or downstream (elongation of the linker; +1 to +10 A.A.) one-by-one per residue. In the reduced mutants (−1 to −10 A.A.), the amino acid residues located upstream of position "0" in the Fig. 1 were just deleted; e.g., the −3 A.A. mutant was designed as -V_{216}-K_{217}-E_{221}-R_{222}-Q_{223}-I_{224}-L_{225}-R_{226}-L_{227}-K_{228}-Q_{229}-I_{230}-. In the elongated mutant (+1 to +10 A.A.), the original sequence was repeatedly inserted at position "0"; e.g., the +5 A.A. mutant was designed as -V_{216}-K_{217}-T_{218}-R_{219}-S_{220}-E-R-Q-I-L-E_{221}-R_{222}-Q_{223}-I_{224}-L_{225}-R_{226}-L_{227}-K_{228}-Q_{229}-I_{230}-. One-by-one analyses of the position-specific deletions/iterations allow for evaluation of the structural properties of the interested region.

Electrophysiology

The cDNAs for WT and mutant mHv1/VSOP channels were transfected into HEK293T cells. The cells were then cultured for 24 h in Dulbecco's modified Eagle's medium supplemented with 10% bovine calf serum. Electrophysiological recordings were performed 4–16 h after reseeding, which corresponded to 18–30 h after transfection. A coverslip with HEK293T cells was placed in a recording chamber containing bath solution (see below) on the stage of an inverted fluorescence microscope (IX71; Olympus), and the transfected cells were identified by the fluorescent signal from the green fluorescent protein. Macroscopic currents were then recorded in the whole cell clamp configuration using an amplifier (Axopatch-200B; Molecular Devices). The pipette resistance in the solution was 3–5 MΩ. 60–80% of the voltage error caused by the series resistance was compensated by a circuit in the amplifier. The recorded currents were low-pass filtered at 2 kHz using a four-pole Bessel filter circuit built into the amplifier. The external solution contained 75 mM NMDG, 1 mM $CaCl_2$, 1 mM $MgCl_2$, 10 mM glucose, and 180 mM HEPES, pH 7.0. The pipette solution contained 65 mM NMDG, 3 mM $MgCl_2$, 1 mM EGTA, and 183 mM HEPES, pH 7.0. Because the activation kinetics depends on the recording temperature (Fujiwara et al., 2012; see Data analysis and Fig. S1), the temperature was controlled (15–45°C) by adding heated or cold external solution to the chamber. Recorded data were analyzed using Clampfit software (Molecular Devices). I-V relationships were analyzed by measuring the current amplitudes at the pulse end of 3-s depolarizations in each mutant (Fig. 1 B). I-V relationships presented were normalized at +100 mV in +10 to −4 A.A., +120 mV in −5 A.A., +140 mV in −6 to −8 A.A., and +160 mV in −9 to −10 A.A., because the thresholds were shifted by the mutations (Fig. 1 B). Thresholds of activation were evaluated by measuring the voltage at which a detectable tail current was elicited. The activation time constant shown in Figs. 1, 2, and S1 was obtained by fitting the activation phase of the outward currents upon depolarization at 100 mV from the onset of the step pulse to the pulse end. Various lengths of pulse time (500 ms, 1 and 3 s) were used to fit the activation phases properly by single-exponential function. Because of the variation of the thresholds of the mutant channels, different membrane potentials were used for analysis for −5 A.A. (analyzed at 120 mV), −6 A.A. (at 140 mV), and −7 A.A. (at 140 mV).

Cross-linking Western blots

To evaluate the positional proximity between the two Hv protomers, cross-linking Western blots were performed (Lee et al., 2008; Fujiwara et al., 2012). The mutant mHv1/VSOP with C103S and C245S was used as a template, where two native Cys residues were mutated to prevent intrinsic disulfide bonds (Cys-less template) (Fujiwara et al., 2013b). The introduction of Cys in the Cys-less template enabled the detection of close positions between two VSDs. Two Cys residues in the transmembrane helices are able to make disulfide bond up to 8 Å apart from each other under the natural oxidization condition (Dmitriev et al., 1999), up to 10–15 Å under the forced oxidation condition (Careaga and Falke, 1992; Wu and Kaback, 1997; Wu et al., 1998; Dmitriev et al., 1999). Hence, the cross-linking approach has been used successfully to examine transmembrane helix proximity (Lainé et al., 2003; Lee et al., 2005; Albright et al., 2007). HEK293T cells were used as the expression host for the mutant channels. Cells were lysed and spun-down with 1% dodecyl maltoside (DDM), and the soluble fraction was used for the cross-linking assay. Suspensions of cells without the DDM treatment were used for the nondetergent assay (Fig. 4 A). Disulfide bonds between two Cys introduced were made by oxidization with Cu-P (mixture of 330 µM $CuSO_4$ and 1 mM O-phenanthroline) for 20 min. A one-hundredth concentration of Cu-P (3.3 µM $CuSO_4$ and 10 µM O-phenanthroline) and 0 mM Cu-P (air oxidation) were also used for the assay (Fig. 4, B and C). The Cu-P reaction was quenched with 5 mM *N*-ethylmaleimide and 50 mM EDTA. Proteins were separated by 12.5% SDS-PAGE under reducing conditions and electrophoretically transferred to Immobilon-P (EMD Millipore). A polyclonal rabbit anti-mHv1/VSOP antibody generated against Met1–Ala72 in the N terminus of mHv1/VSOP was used for detection (Sakata et al., 2010). Horseradish peroxidase–conjugated donkey anti–rabbit IgG (GE Healthcare) was used as the secondary antibody. To analyze the amount of proteins (cross-linked and un–cross-linked), intensities of bands on the gel were measured with a high dynamic range (16,000 gray level) by the CS analyzer system (version 3; ATTO Corp.). Because intensities of the Western blot bands were varied by trial, we did not compare them directly but analyzed the ratio of cross-linking (see Data analysis).

Data analysis

To evaluate the activation kinetics of the linker mutants, an inverse logarithm (Log (1/τ)) of the activation time constant (τ) was calculated and plotted versus temperature (Fujiwara et al., 2012) (Fig. S1). The plotted data were fitted by linear regression with error variances. Individual average values on the fitting lines at 3.30×10^{-3} K^{-1} (30.0°C) were used for the Fourier transform methods.

To evaluate the ratio of cross-linking, intensities of two bands in the cross-linking Western blot were analyzed. Two bands, cross-linked and uncross-linked, were observed after the cross-linking by Cu-P, and we assumed two components of protein conformation. The relative ratio (*rR*) of cross-linking was calculated by the following equation (Hessa et al., 2005):

$$rR = -\mathrm{RT}\ln\left(\mathrm{I}_{x2} / \mathrm{I}_{x1}\right),$$

where I_{X1} is the intensity for the uncross-linked band, I_{X2} is the intensity for the cross-linked band, R is the gas constant, and T is the absolute temperature. The calculated *rR* were normalized by subtracting the background cross-link,

$$\left|rR_{\mathrm{cys}}\right| = -\left(rR - rR_{\mathrm{cysless}}\right),$$

where rR_{cysless} is the relative ratio calculated by the background intensity with the Cys-less mutant (C103S and C245S). Individual $|rR_{\mathrm{cys}}|$ values were used for the Fourier transform methods.

For the analyses of the periodicity of the data variation, we used the Fourier transform methods (Cornette et al., 1987; Rees et al., 1989; Perozo et al., 1998, 1999; Minor et al., 1999; Li-Smerin et al., 2000; Dalmas et al., 2010). The power spectrum, P (ω), is calculated from the following equation:

$$\mathrm{P}(\omega) = \left\{\sum_{k=0}^{l-1}\left(h_k - \bar{h}\right)\cos k\omega\right\}^2 + \left\{\sum_{k=0}^{l-1}\left(h_k - \bar{h}\right)\sin k\omega\right\}^2, \quad \bar{h} = \left(\sum_{k=0}^{l-1} h_k\right) / l,$$

where ω is frequency, h_k is the individual data, and l is the protein segment of length (number of A.A. residue). To evaluate the probability that the protein folds in α helix, the following equation was used:

$$\alpha\mathrm{PI} = \frac{\frac{1}{40}\int_{80^\circ}^{120^\circ}\mathrm{P}(\omega)\,\mathrm{d}\omega}{\frac{1}{180}\int_{0^\circ}^{180^\circ}\mathrm{P}(\omega)\,\mathrm{d}\omega},$$

where α-PI > 2.0 is a strong indication of α-helical secondary structure (Cornette et al., 1987; Rees et al., 1989).

The data were analyzed using Igor Pro (WaveMetrics, Inc), Excel (Microsoft), and Kyplot (KyensLab Inc.) software.

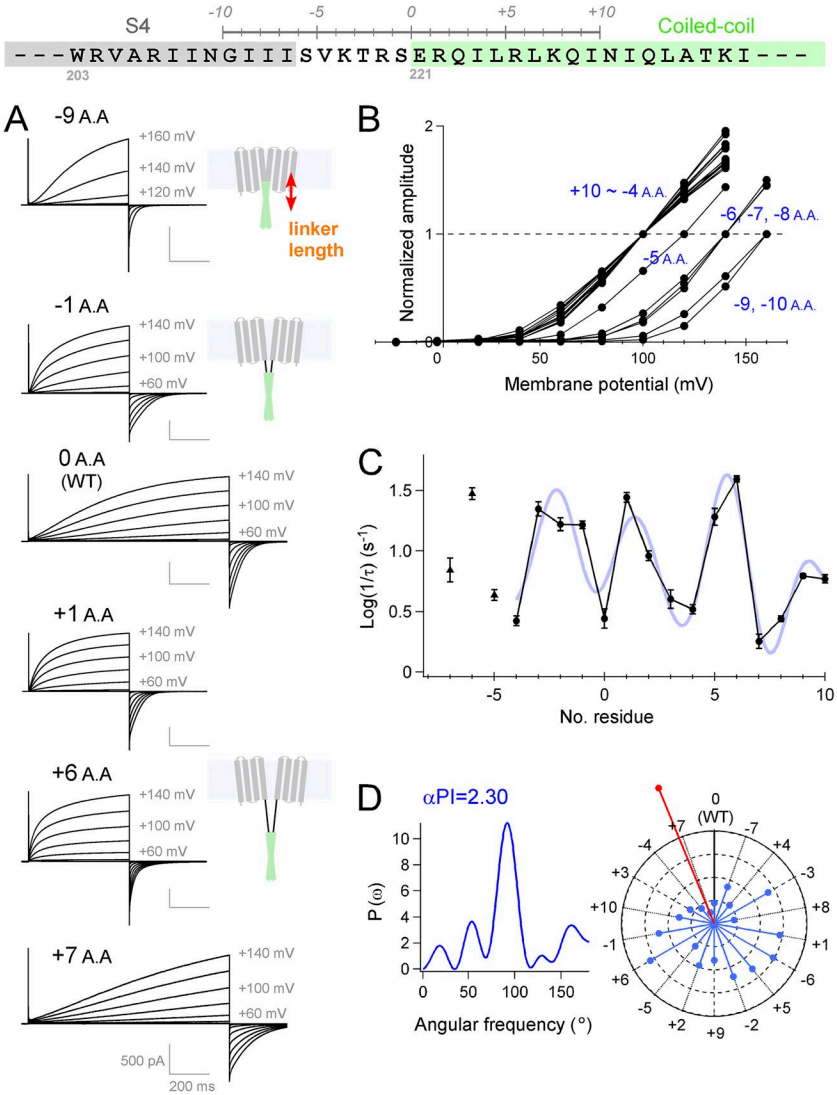

Figure 1. Analysis of the interdomain interactions between the transmembrane and the cytoplasmic domains. (A) Experimental strategy for changing the linker length and the representative current traces of the mutants recorded at 25°C. Our previous crystal structure analysis for the coiled-coil domain protein (S220-N269) (Fujiwara et al., 2012) showed that an α helix starts from E221 (light green box). (B) Normalized I-V relationship of WT (0 A.A.) and the mutant channels. I-V relationships of the 15 mutants (+10 to −4 A.A.) have an overlap with each other. (C) Accumulated data of activation kinetics of each mutant are plotted against the linker length. A Fourier series fitting to the data (+10 to −4 A.A.) is also indicated (light blue curve). The data were plotted as the mean ± error variance. (D) Power spectrum of the Fourier transform of the data (+10 to −4 A.A.) and the helical wheel diagrams. Vectors (light blue) indicate the activation time constant (Log (1/τ)) of the mutants, and the inverse direction of the sum vector (red) is also indicated. Details of the data analysis are described in Materials and methods.

Phase angle calculation and structure modeling

Phase angles were calculated with the TWISTER program (Strelkov and Burkhard, 2002). The coiled-coil structure is generally twisted and the residues composing the core face each other, which restricts the phase angle of the hydrophobic position "a" in the range of 25–30° in the homodimer coiled-coil. The structure model was built with the crystal structure of the VSD of Kv and Nav (Long et al., 2005; Payandeh et al., 2011) and the coiled-coil domain of Hv (Fujiwara et al., 2012). We note that W203 in the structure model is located beside the S3 helix in the model. An aromatic residue, F, in the middle of S4 is also situated in the same fashion in other VSDs of Kv and Nav (Long et al., 2005; Payandeh et al., 2011).

Online supplemental material

Fig. S1 indicates full datasets of the electrophysiological analysis with the linker mutants (−10 A.A. to +10 A.A.). Fig. S2 shows that further reduction of the linker made the channel nonfunctional. Fig. S3 illustrates the predicted orientation of the transmembrane segments coordinated with the coiled-coil domain in the linker mutants. Fig. S4 shows full datasets of the cross-linking experiments for the transmembrane region. Fig. S5 demonstrates that cross-links between the two S4s occurred at the intersubunit interface. Fig. S6 illustrates two different models of the transmembrane orientation, with a discussion of the gating motion. The online supplemental material is available at http://www.jgp.org/cgi/content/full/jgp.201311082/DC1.

RESULTS

Functional interaction between the transmembrane and cytoplasmic domains

To analyze the interdomain interaction between the coiled-coil domain and the VSD, we targeted the linker region between them. We constructed and analyzed a series of linker mutant channels, where the coiled-coil domain was shifted upstream (reduction of the linker length; −1 to −10 A.A.) or downstream (elongation of the linker; +1 to +10 A.A.) one-by-one per residue (Fig. 1 A; Materials and methods and Fig. S1). In the elongated mutants, the original sequence was repeatedly inserted (see Materials and methods). All mutant channels showed functional currents, and the thresholds of the activation shifted gradually toward positive direction by significant reductions of the linker length (greater than or equal to −5 A.A.) (Fig. 1 B). By further reduction of the linker (greater than −10 A.A.), the channels did not show enough current amplitude to analyze accurately where the −11-A.A. mutant showed a drastic shift of the activation threshold, and currents of the −12-A.A. and the −13-A.A. mutants are no longer detected (Fig. S2). We also found that the activation kinetics showed variations commensurate with the length of the linker. Activation kinetics of mouse Hv reportedly reflects the cooperative channel gating that makes activation slower (i.e., more sigmoidal), and the fast activation coincides with the loss of cooperativity observed in the monomeric channel (Gonzalez et al., 2010; Fujiwara et al., 2013a). We observed that even a single residue reduction or increase of the linker length accelerated the activation kinetics significantly (Fig. 1 A, −1 A.A. and +1 A.A.), whereas the slow activation kinetics observed in the WT channel recovered in other mutants (Fig. 1 A, +7 A.A.). The activation kinetics of the mutants, plotted against the linker length, showed clear periodicity (Fig. 1 C). We examined the data (+10 to −4 A.A.) using Fourier transform methods (Cornette et al., 1987; Rees et al., 1989; Perozo et al., 1998, 1999; Minor et al., 1999; Li-Smerin et al., 2000; Dalmas et al., 2010) (see Materials and methods). The strongest peak in the power spectrum occurs at 95°, a frequency within the characteristic range for an α helix (Fig. 1 D). α-PI was calculated to be 2.30, exceeding a value of 2.0, which has been reported to be a criteria of the α-helical secondary structure (Cornette et al., 1987; Rees et al., 1989). Therefore, the coiled-coil domain and the transmembrane VSD have a functional interaction in the helical periodicity. Individual values of activation

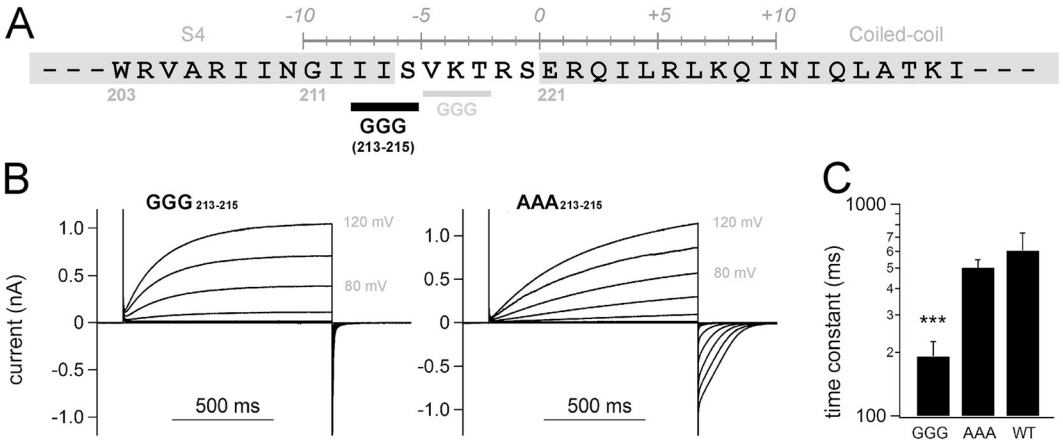

Figure 2. Electrophysiological analysis of the GGG/AAA mutants. (A) Position of the Gly_{213}-Gly_{214}-Gly_{215} mutation is indicated (black bold), as is that of the previous $GGG_{216–218}$ mutation in the earlier study (Fujiwara et al., 2012) (gray). (B) Representative current traces of the mutants at 25°C. (C) Accumulated data of activation kinetics of the mutant are shown as the mean ± SEM ($n = 5$ in the GGG mutant, $n = 6$ in the AAA mutant, and $n = 5$ in WT). ***, $P < 0.001$, paired t test between GGG versus AAA.

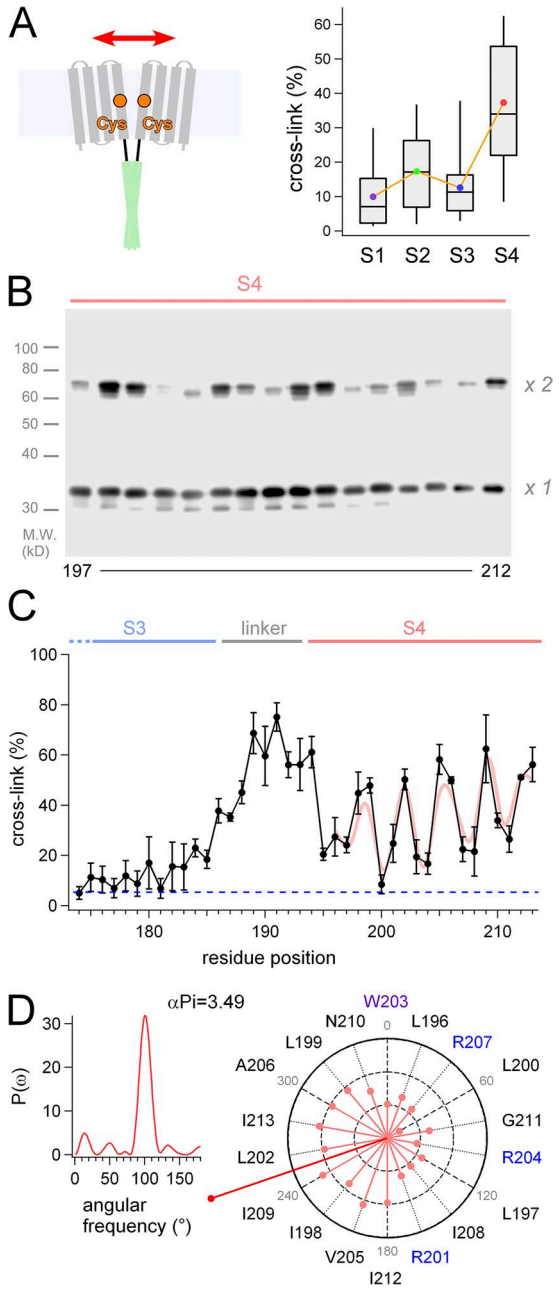

Figure 3. Analysis of the interdomain interaction between two transmembrane VSDs. (A) Experimental strategy for the cross-linking Western blots by disulfide bonds (left), and the box plot for the cross-linking of each transmembrane segment (right). Bars indicate maximum/minimum, and boxes denote interquartile ranges for the individual transmembrane segments. Averaged data are plotted as color dots. (B) A representative image of the Western blot analysis for the S4 segment. Channels that are cross-linked by an interdomain disulfide bond show twice the molecular weight of monomer on the gel (×2 vs. ×1). (C) Accumulated data of the cross-linking analysis and a Fourier series fitting to the data (light red curve). The data were plotted as the mean ± SEM ($n = 3$). A blue dashed line indicates background signal of the negative control in this analysis. (D) Power spectrum of the Fourier transform of the data (197–212) and the helical wheel diagrams. Vectors (light red) indicate $|rR_{cys}|$ for each Cys position introduced, and the sum vector (deep red) is indicated.

kinetics are plotted in the helical wheel diagram as vectors (Fig. 1 D). Distribution of the vectors shows clear predisposition, and the inverse sum vector (red vector) points the direction of the slowest activation (Fig. 1 D). This suggests that the channels show slow activation kinetics when the connection between the coiled-coil domain and the transmembrane VSD is in the same torsion to that of WT (Fig. S3).

We also observed that introduction of the $GGG_{213–215}$ mutation into the joint region between S4 and the linker accelerated the channel gating, whereas the $AAA_{213–215}$ mutant did not show clear differences from WT (Fig. 2), which was consistent with our previous results of the $GGG_{216–218}/AAA_{216–218}$ mutation into the linker (Fujiwara et al., 2012). As the introduction of Ala in the helix is known to retain the helical folding (O'Neil and DeGrado, 1990; Chakrabartty et al., 1991; Findeisen and Minor, 2009; Fujiwara et al., 2012), we assumed that the linker region including the end of S4 (residues 212–220) is likely to form an α helix throughout its length. Thus, the transmembrane S4 helix and the cytoplasmic coiled-coil domain showed an α-helical interaction in the channel gaiting, which conjures an image of the continuous structural basis of α helix between S4 and the coiled-coil.

Positional proximity between two transmembrane domains

We next tried to address how the interface between two transmembrane VSDs is formed and supported by the coiled-coil structure (Fig. 3 A). We used the cross-linking Western blot assay (Careaga and Falke, 1992; Wu and Kaback, 1997; Wu et al., 1998; Dmitriev et al., 1999; Lainé et al., 2003; Lee et al., 2005, 2008) to detect an intersubunit disulfide bond that is formed by Cys introduced in the transmembrane region (residues 98–213). The ratios of cross-link were obtained by measuring the signal intensity of two bands: ×1 and ×2 of molecular weights (Figs. 3 B and S4). The average cross-link for each of the transmembrane segments (S1–S4) is summarized in Fig. 3 A, indicating that the ratios for the S4 segment were higher than those for other segments (Fig. 3 A). Ratios for the loops between each transmembrane segment (S1–S2, S2–S3, and S3–S4) were basically high (Fig. S4), which might be caused by some protein flexibility. Flexible or unfolded segments, in some cases, make it difficult to estimate the structural proximity; we were not able to evaluate the data for the loops. On the other hand, the cross-linking approach for the membrane-spanning helices has been used successfully to examine the helix proximity (Careaga and Falke, 1992; Wu and Kaback, 1997; Wu et al., 1998; Dmitriev et al., 1999; Lainé et al., 2003; Lee et al., 2005). Cross-linking ratios were plotted against the mutation sites, and we found a periodicity in the variation (Fig. 3 C). Assuming two components of protein conformation caused by the disulfide bond, relative ratios of cross-linking ($|rR_{cys}|$) for

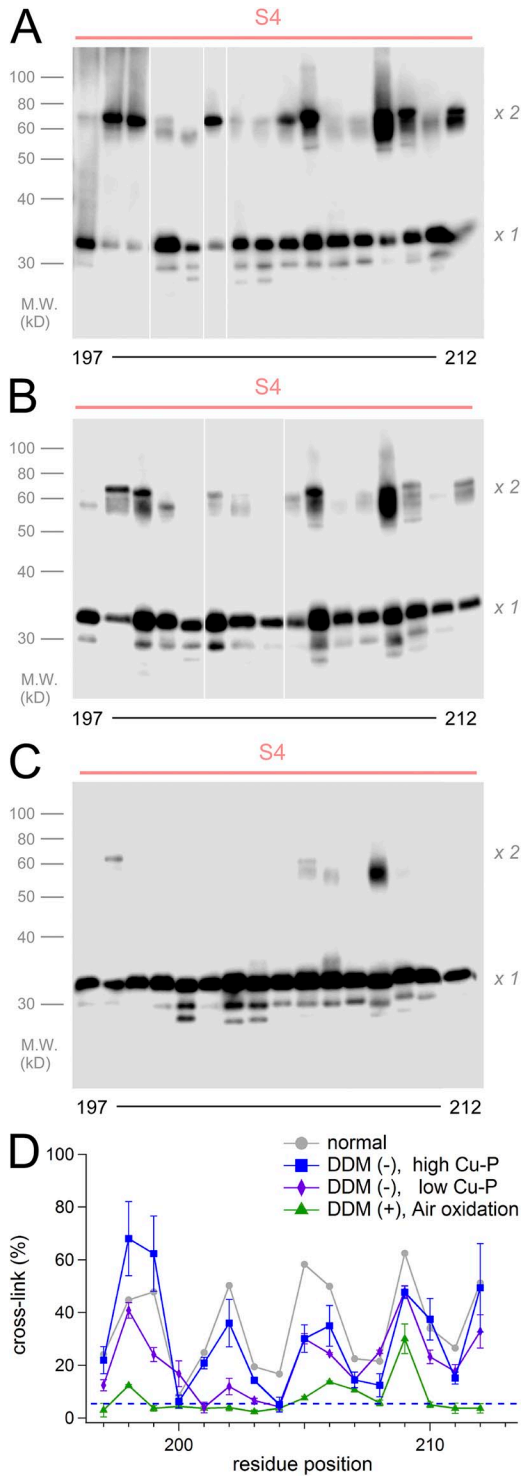

Figure 4. Cross-linking analysis for S4 in various conditions. (A–C) Representative images of the cross-linking analysis for the S4 segment. Suspensions of cells in the absence of DDM were analyzed (A and B). Cross-links were induced by Cu-P (A), by 100th concentration of Cu-P (B), and by the air oxidation (C). White lines in A and B indicate that intervening lanes have been spliced out. (D) Accumulated data of the cross-linking analysis. The data were plotted as the mean ± SEM ($n = 3$). The gray line indicates the control data in the normal condition (DDM (+) and Cu-P (+)) from Fig. 3 C. The blue dashed line indicates background signal of the negative control in this analysis.

each residue position were calculated (see Materials and methods). Analysis (residues 197–212) using Fourier transform methods showed that the strongest peak in the power spectrum occurs at 101° (α-PI = 3.49), a frequency within the characteristic range for an α helix. Individual $|rR_{cys}|$ values were plotted as vectors on a helical wheel, which showed a clear predisposition of the periodicity (Fig. 3 D). The sum vector (Fig. 3 D, deep red) therefore points to the side where residues have the largest cross-linking ratio, identifying the face involved in protein–protein interactions in the dimeric VSDs. It is also notable that the interaction between two S4 helices was found over a sufficient range of length, suggesting that two parallel S4 helices would have a line contact to each other.

We examined influence of the detergent and the oxidant in the cross-linking (Fig. 4). Cross-links for the S4 region were still observed in the absence of the DDM treatment, and the ratios were not changed essentially (Fig. 4, A and D). Cross-linking ratios were decreased in the mild oxidation condition, especially in the middle range of the S4 segment (Fig. 4, B and D). Cross-links were rarely observed by air oxidation (Fig. 4, C and D). Thus, S4 helices that existed in the membrane were able to make cross-links to each other. The finding that the weak air oxidation was almost ineffective (Fig. 4 C) suggested that cross-links observed in Fig. 4 (A and B) were formed in the lipid environment, which is consistent with the direction of the interaction interface between two S4 helices (Fig. 3 D). We also performed the cross-linking assay for the S4 segment with monomeric and tandem channel mutants, which demonstrates that the cross-links between the two S4s occurred at the intersubunit interface (Fig. S5).

We also examined the cross-link between the S4 helices in the linker mutants, which were analyzed in Fig. 1. High ratios of cross-link were observed in the +7-A.A. mutant showing slow activation as that of WT (Fig. 5 A), and the helical wheel diagram indicated a similar direction of the sum vector to that of WT (Fig. 5, D and E). On the contrary, the extent of cross-link of the −1-A.A. mutant showing fast activation kinetics was significantly diminished (Fig. 5 B). Cross-links of the +1-A.A mutant showing fast activation kinetics was also decreased largely, and some minor bands at 203 and 210 were newly observed (Fig. 5 C), suggesting that the periodicity of the +1-A.A. mutant appeared to be shifted downstream by one residue. We considered that this might reflect a rotational movement of the S4 region by the one-residue shift of the coiled-coil (Fig. S3). Thus, two VSDs in the membrane have an orientation with the close interface between two S4 helices, which is important for establishing the gating cooperativity.

Spatial relationships among two VSDs and a coiled-coil

We analyzed the domain–domain interaction of the Hv dimer, and the data indicated α-helical periodicity

in both cases of the interaction between the VSD and the coiled-coil (Fig. 1), and the interaction between two VSDs (Fig. 3). Consistency of the data (Figs. 1 and 3) was examined with structure modeling of S4 and the coiled-coil. The amino acid sequence of the S4 segment and the coiled-coil domain is well conserved among species (Fig. 6 A). A conserved W203 is used here as a landmark for the structural orientation (Fig. 6 A). W203 is just 21 residues, 6 helix turns (3-heptad), upstream from I224, the initial residue of the coiled-coil core. The structural orientation of the coiled-coil is defined by its hydrophobic core, in which two hydrophobic residues of heptad form the core with regularity, and each Cα position of the residues is defined with a phase angle to the central axis (Crick, 1953). Based on the crystal structure of the coiled-coil of Hv (Fujiwara et al., 2012), the initial phase angle at I224 (Φ) is 27° (Fig. 6 B, left). Once the coiled-coil is untwisted, the phase angle rotates 20° per heptad clockwise along the straight α helix to the upstream. The phase angle at W203 is calculated to be 87° based on the 3-heptad shift (20° × 3) from I224 along straight α helices (Fig. 6 B, left). Thus, based on the assumption of the continuous α helices (Fig. 1), W203 in each S4 was positioned separately from each other (Fig. 6 B). This position, in fact, nicely fits the results of the cross-linking; i.e., the cross-linking ratio of W203 was low and the helical wheel diagram points to W203 at twelve o'clock (Fig. 3). In addition, positions showing the high cross-linking ratio (orange marks) between the two S4s were favorably aligned face-to-face (Fig. 6 B). Meanwhile, as Asn and Gly are known to have flexibility in a helix, there is an alternative possibility that a proposed continuous helix is broken at N210 and G211 (Fig. 6 B). In that case, the upstream region from N210 would show an inconsistency between the cross-linking ratio and the phase angle, but it does not match the results. Although breaking or kinking at this point might exist in some state of the channel function, the results from biochemical and functional approaches in our experimental conditions coherently support the idea of the continuous α helices.

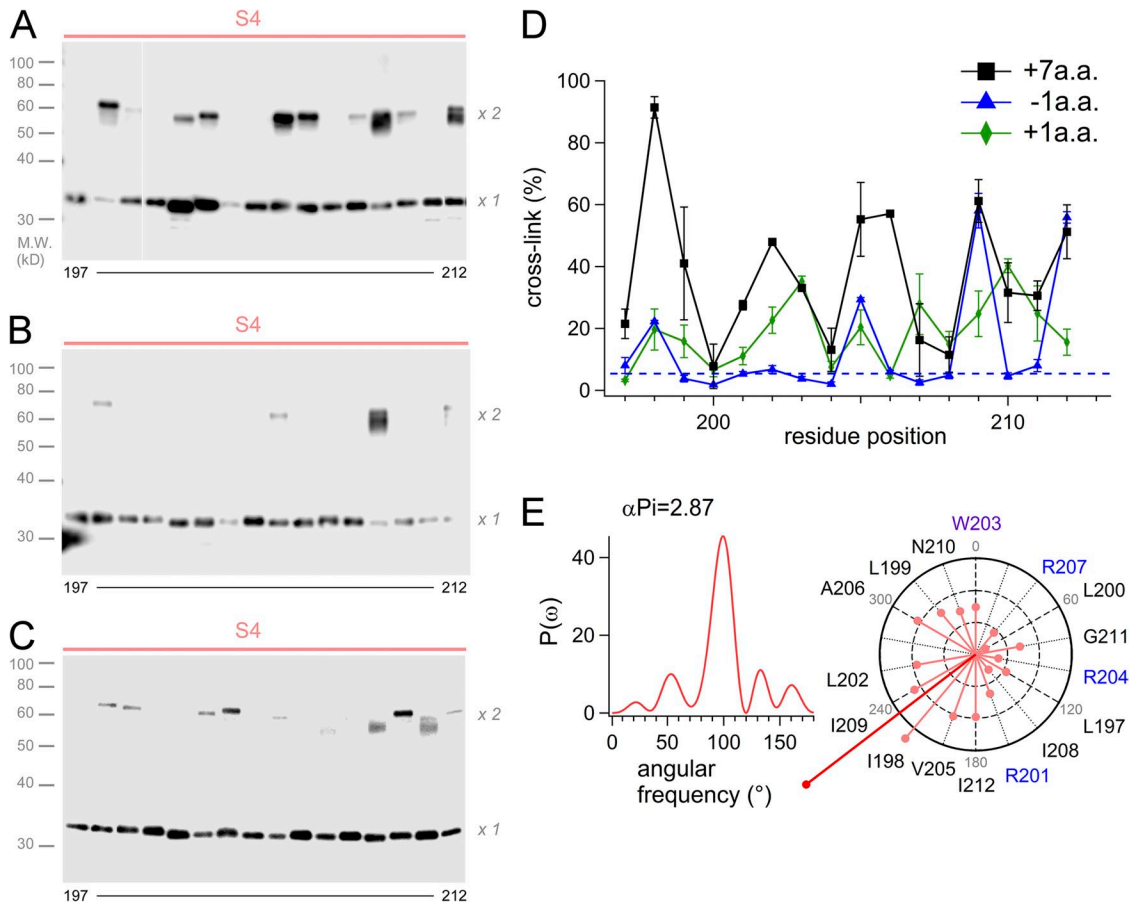

Figure 5. Cross-linking analysis of the mutants by Western blot. (A–C) Representative images of the Western blot analysis for the S4 segment of the +7-A.A. mutant (A), the −1-A.A. mutant (B), and the +1-A.A. mutant (C). White line in A indicate that intervening lanes have been spliced out. (D) Accumulated data of the cross-linking analysis for the linker mutant channels. The data were plotted as the mean ± SEM ($n = 3$). (E) The power spectrum of the Fourier transform of the data (197–212) and the helical wheel diagrams for the +7-A.A. mutant. The sum vector (deep red) indicated points the same direction to that of WT shown in Fig. 3 D.

DISCUSSION

In this study, we focused on the interdomain interactions among two VSDs and a coiled-coil domain, and analyzed the functional couplings and the positional proximity among domains. Systematic mutations of the linker region between S4 of VSD and the coiled-coil showed that the channel gating was altered in the helical periodicity with linker length, suggesting that two domains are linked by helices (Figs. 1 and 2). Cross-linking analyses revealed that the two S4 helices were situated closely in the dimeric channel (Figs. 3 and 4), which is also involved in the gating property (Fig. 5).

Cross-linking analysis for the human Hv has also been performed previously (Lee et al., 2008). Lee et al. examined the cross-links for 15 sites that were selected using the voltage sensor of the Kv1.2–Kv2.1 paddle chimera structure as a reference. They succeeded in identifying strong cross-linking sites in the S1–S2 loop (L120-E124 in the mouse sequence), and also identified the weak cross-linking position at the end of S1 (L116), suggesting that the structural model in which extracellular ends of S1 helices have contact with each other. They also identified weak cross-linking positions in the S2–S3 loop (L169) and in the S3–S4 loop (H190). All of them were repeatedly observed in our present study. L199 (L203 in the human sequence), a highly cross-linked site in our study, did not show cross-linking bands in the previous study (Lee et al., 2008). This may be because of a methodological difference along with the species or a difference in preparation of samples: Lee et al. (2008) analyzed membrane fractions with ultrasonic breaking and ultracentrifugation. Actually, in positions near the lipid–water interfaces, the cross-links are hard to evaluate because of the issues of the detergent solubilization, the protein flexibility, and the oxidant accessibility. Our recent analysis of the accessibility of cysteine-modifying reagents to

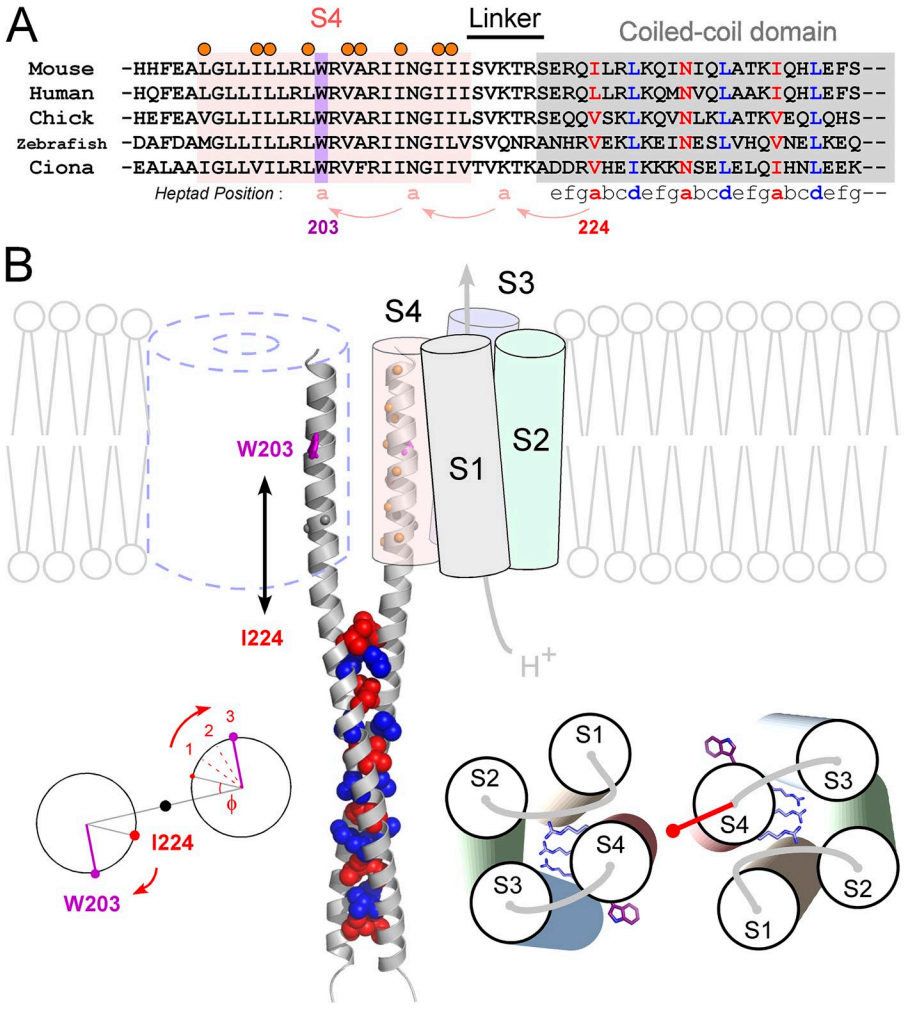

Figure 6. Molecular architecture of the dimeric Hv. (A) Sequence alignment of S4 and the C-terminal cytoplasmic coiled-coil domain of Hv from various species. Positions of the coiled-coil heptad repeat (*abcdefg*) are indicated below the alignment (Lupas, 1996; Burkhard et al., 2001). Coiled-coil residues occupying hydrophobic "a" and "d" positions are denoted by blue and red, respectively. The conserved W203 in S4 is highlighted in violet. Positions showing high cross-linking ratios (Fig. 3) are marked by orange circles. (B) A model of the Hv dimer based on the experimental data and the crystal structures of the coiled-coil domain of Hv (Fujiwara et al., 2012) and VSD of Kv (Long et al., 2005). Spheres depicting the core residues of "a" (red) and "d" (blue) positions of the coiled-coil on ribbon backbones (gray) are shown. W203 and orange balls depicting the residues showing the high cross-linking ratio are shown on the continuous helix ribbon backbones from the coiled-coil. N210 and Gly211 (gray balls) are also highlighted because of an alternative model in which a continuous helix might be broken here. Calculation of the phase angle at W203, which is 21 residues, 3-heptad, upstream of I224 (left). The model for the helix orientation of the VSD based on the cross-linking (right). Three conserved Arg's and W203s are shown as sticks. The red vector depicts the sum vector of Fig. 3 D. In this study, the transmembrane region, i.e., the S4 segment, was defined based on the sequence alignment with the Kv family and the hydrophobicity profile of the S4 segment. The observation that the gradual shift of the threshold by decrease of the linker length (greater than or equal to −5 A.A.) (Fig. 1 B) might be caused by the hydrophobic mismatch between the lipid membrane and the coiled-coil domain, of which surface residues are hydolophilic, in addition to the interpretation of the restriction of the S4 movement by the coiled-coil.

the whole transmembrane region showed high accessibility at positions near the lipid–water interfaces (Kurokawa and Okamura, 2014). L199 is located in the lipid–water interface. In addition, the α-helical periodicity for S4 observed in the present study is not explained by the position-specific difference of the accessibility.

The structure model (Fig. 6 B) shows uniqueness when compared with other VSD structures of Kv and Nav, which are known to be in an activated state (Long et al., 2005; Payandeh et al., 2011). The long-distance interaction between two S4s (Fig. 3) indicates that the S4 helix of Hv is more perpendicular to the membrane than that of other VSD structures (Long et al., 2005; Payandeh et al., 2011) (Fig. 6 B). Besides, all analyzed data in this study did not show 3_{10}-helical periodicity (120°) but an α-helical one (100°), unlike Kv (Long et al., 2005; Villalba-Galea et al., 2008) and Nav (Payandeh et al., 2011), in which a part of S4 folds in 3_{10}-helix. In addition, the cross-linking ratio for the S1–S4 region did not reach full scores with high Cu-P, mostly ∼50% for the strong cross-linking sites, whereas the ratio for C245 in the rigid coiled-coil domain was almost 100% (Fig. S4, A and B). This partial cross-link could be caused by a certain level of structural mobility in the transmembrane region. In fact, a preceding study proposed a different model for the human Hv dimer, in which extracellular ends of S1 helices are close to each other based on the cross-linking data (Lee et al., 2008). If some rotational movements of VSD occur during the channel gating, the interaction interface between two VSDs could be switched (Fig. S6). The significant reduction of cross-link for S4 in the −1-A.A. mutant, with the accompanying altered activation (Fig. 5 E), supports the possible rearrangement of the S4–S4 configuration during the gating. A recent study of voltage-clamp fluorometry also suggested the rearrangement of helix configuration during the gating (Qiu et al., 2013). The model in Fig. 6 B most likely reflects a closed state, because the cross-linking experiments were performed at 0 mV (Fig. 3), and the activation kinetics largely reflects the condition of closed states (Fig. 1). Thus, the Hv dimer has a unique protein architecture, in which two movable VSDs for the gating are supposed to be tied by the long helices twisting into a coiled-coil in the cytoplasm. In this view, the activation threshold raised by the reduction (greater than or equal to −5 A.A.) of the linker length (Figs. 1 B and S2) could be interpreted as physical restriction of the S4 movement (rearrangement) during the gating. The potential flexibility around N210 and G211 might have relation to the gating. Because of the adjacency of two S4s, spatial constraint of the S4 movement such as rotating or sliding during the gating (Bezanilla, 2000) might result in the gating cooperativity, which manifests as the slow activation (Fig. 1). In sum, functional cores for voltage sensing and subunit assembly are directly linked beyond the plasma membrane, forming a rigid structural basis for the cooperative function.

We would like to thank Ms. M. Kobayashi and Ms. S. Ieki for technical assistance. We would like to thank Drs. Y. Sako (Institute of Physical and Chemical Research, Wako, Japan), F. Ono (National Institute on Alcohol Abuse and Alcoholism, Rockville, MD), and J. Cui (Washington University, St. Louis, MO) for commenting on the manuscript.

This work was supported by grants from Japan Society for the Promotion of Science (KAKENHI: 21770171 to T. Kurokawa, 23136510 and 25136713 to Y. Fujiwara, and 25253016 to Y. Okamura) and the Naito foundation (to Y. Fujiwara).

The authors declare no competing financial interests.

Author contributions: Y. Fujiwara and T. Kurokawa designed the experiments; Y. Fujiwara performed the electrophysiological experiments; Y. Fujiwara and T. Kurokawa performed the biochemical analyses; and Y. Fujiwara and Y. Okamura wrote the paper.

Kenton J. Swartz served as editor.

Submitted: 7 August 2013
Accepted: 22 January 2014

REFERENCES

Albright, R.A., K. Joh, and J.H. Morais-Cabral. 2007. Probing the structure of the dimeric KtrB membrane protein. *J. Biol. Chem.* 282:35046–35055. http://dx.doi.org/10.1074/jbc.M704260200

Armstrong, C.M., and B. Hille. 1998. Voltage-gated ion channels and electrical excitability. *Neuron.* 20:371–380. http://dx.doi.org/10.1016/S0896-6273(00)80981-2

Bezanilla, F. 2000. The voltage sensor in voltage-dependent ion channels. *Physiol. Rev.* 80:555–592.

Burkhard, P., J. Stetefeld, and S.V. Strelkov. 2001. Coiled coils: a highly versatile protein folding motif. *Trends Cell Biol.* 11:82–88. http://dx.doi.org/10.1016/S0962-8924(00)01898-5

Careaga, C.L., and J.J. Falke. 1992. Thermal motions of surface α-helices in the D-galactose chemosensory receptor. Detection by disulfide trapping. *J. Mol. Biol.* 226:1219–1235. http://dx.doi.org/10.1016/0022-2836(92)91063-U

Chakrabartty, A., J.A. Schellman, and R.L. Baldwin. 1991. Large differences in the helix propensities of alanine and glycine. *Nature.* 351:586–588. http://dx.doi.org/10.1038/351586a0

Cornette, J.L., K.B. Cease, H. Margalit, J.L. Spouge, J.A. Berzofsky, and C. DeLisi. 1987. Hydrophobicity scales and computational techniques for detecting amphipathic structures in proteins. *J. Mol. Biol.* 195:659–685. http://dx.doi.org/10.1016/0022-2836(87)90189-6

Crick, F.H.C. 1953. The packing of α-helices: simple coiled-coils. *Acta Crystallogr.* 6:689–697. http://dx.doi.org/10.1107/S0365110X53001964

Dalmas, O., L.G. Cuello, V. Jogini, D.M. Cortes, B. Roux, and E. Perozo. 2010. Structural dynamics of the magnesium-bound conformation of CorA in a lipid bilayer. *Structure.* 18:868–878. http://dx.doi.org/10.1016/j.str.2010.04.009

Decoursey, T.E. 2003. Voltage-gated proton channels and other proton transfer pathways. *Physiol. Rev.* 83:475–579.

Dmitriev, O., P.C. Jones, W. Jiang, and R.H. Fillingame. 1999. Structure of the membrane domain of subunit *b* of the *Escherichia coli* F_0F_1 ATP synthase. *J. Biol. Chem.* 274:15598–15604. http://dx.doi.org/10.1074/jbc.274.22.15598

El Chemaly, A., Y. Okochi, M. Sasaki, S. Arnaudeau, Y. Okamura, and N. Demaurex. 2010. VSOP/Hv1 proton channels sustain calcium entry, neutrophil migration, and superoxide production by limiting cell depolarization and acidification. *J. Exp. Med.* 207:129–139. http://dx.doi.org/10.1084/jem.20091837

Findeisen, F., and D.L. Minor Jr. 2009. Disruption of the IS6-AID linker affects voltage-gated calcium channel inactivation and facilitation. *J. Gen. Physiol.* 133:327–343. http://dx.doi.org/10.1085/jgp.200810143

Fujiwara, Y., T. Kurokawa, K. Takeshita, M. Kobayashi, Y. Okochi, A. Nakagawa, and Y. Okamura. 2012. The cytoplasmic coiled-coil mediates cooperative gating temperature sensitivity in the voltage-gated H^+ channel Hv1. *Nat Commun.* 3:816. http://dx.doi.org/10.1038/ncomms1823

Fujiwara, Y., T. Kurokawa, K. Takeshita, A. Nakagawa, H.P. Larsson, and Y. Okamura. 2013a. Gating of the designed trimeric/tetrameric voltage-gated H^+ channel. *J. Physiol.* 591:627–640. http://dx.doi.org/10.1113/jphysiol.2012.243006

Fujiwara, Y., K. Takeshita, A. Nakagawa, and Y. Okamura. 2013b. Structural characteristics of the redox-sensing coiled coil in the voltage-gated H^+ channel. *J. Biol. Chem.* 288:17968–17975. http://dx.doi.org/10.1074/jbc.M113.459024

Gonzalez, C., H.P. Koch, B.M. Drum, and H.P. Larsson. 2010. Strong cooperativity between subunits in voltage-gated proton channels. *Nat. Struct. Mol. Biol.* 17:51–56. http://dx.doi.org/10.1038/nsmb.1739

Hessa, T., H. Kim, K. Bihlmaier, C. Lundin, J. Boekel, H. Andersson, I. Nilsson, S.H. White, and G. von Heijne. 2005. Recognition of transmembrane helices by the endoplasmic reticulum translocon. *Nature.* 433:377–381. http://dx.doi.org/10.1038/nature03216

Jan, L.Y., and Y.N. Jan. 2012. Voltage-gated potassium channels and the diversity of electrical signalling. *J. Physiol.* 590:2591–2599. http://dx.doi.org/10.1113/jphysiol.2011.224212

Koch, H.P., T. Kurokawa, Y. Okochi, M. Sasaki, Y. Okamura, and H.P. Larsson. 2008. Multimeric nature of voltage-gated proton channels. *Proc. Natl. Acad. Sci. USA.* 105:9111–9116. http://dx.doi.org/10.1073/pnas.0801553105

Kurokawa, T., and Y. Okamura. 2014. Mapping of sites facing aqueous environment of voltage-gated proton channel at resting state: A study with PEGylation protection. *Biochim. Biophys. Acta.* 1838:382–387. http://dx.doi.org/10.1016/j.bbamem.2013.10.001

Lainé, M., M.C. Lin, J.P. Bannister, W.R. Silverman, A.F. Mock, B. Roux, and D.M. Papazian. 2003. Atomic proximity between S4 segment and pore domain in Shaker potassium channels. *Neuron.* 39:467–481. http://dx.doi.org/10.1016/S0896-6273(03)00468-9

Lee, S.Y., A. Lee, J. Chen, and R. MacKinnon. 2005. Structure of the KvAP voltage-dependent K^+ channel and its dependence on the lipid membrane. *Proc. Natl. Acad. Sci. USA.* 102:15441–15446. http://dx.doi.org/10.1073/pnas.0507651102

Lee, S.Y., J.A. Letts, and R. Mackinnon. 2008. Dimeric subunit stoichiometry of the human voltage-dependent proton channel Hv1. *Proc. Natl. Acad. Sci. USA.* 105:7692–7695. http://dx.doi.org/10.1073/pnas.0803277105

Li-Smerin, Y., D.H. Hackos, and K.J. Swartz. 2000. α-helical structural elements within the voltage-sensing domains of a K^+ channel. *J. Gen. Physiol.* 115:33–50. http://dx.doi.org/10.1085/jgp.115.1.33

Lishko, P.V., I.L. Botchkina, A. Fedorenko, and Y. Kirichok. 2010. Acid extrusion from human spermatozoa is mediated by flagellar voltage-gated proton channel. *Cell.* 140:327–337. http://dx.doi.org/10.1016/j.cell.2009.12.053

Long, S.B., E.B. Campbell, and R. Mackinnon. 2005. Crystal structure of a mammalian voltage-dependent Shaker family K^+ channel. *Science.* 309:897–903. http://dx.doi.org/10.1126/science.1116269

Lupas, A. 1996. Coiled coils: new structures and new functions. *Trends Biochem. Sci.* 21:375–382.

Minor, D.L., Jr., S.J. Masseling, Y.N. Jan, and L.Y. Jan. 1999. Transmembrane structure of an inwardly rectifying potassium channel. *Cell.* 96:879–891. http://dx.doi.org/10.1016/S0092-8674(00)80597-8

Musset, B., S.M. Smith, S. Rajan, V.V. Cherny, S. Sujai, D. Morgan, and T.E. DeCoursey. 2010. Zinc inhibition of monomeric and dimeric proton channels suggests cooperative gating. *J. Physiol.* 588:1435–1449. http://dx.doi.org/10.1113/jphysiol.2010.188318

O'Neil, K.T., and W.F. DeGrado. 1990. A thermodynamic scale for the helix-forming tendencies of the commonly occurring amino acids. *Science.* 250:646–651. http://dx.doi.org/10.1126/science.2237415

Okochi, Y., M. Sasaki, H. Iwasaki, and Y. Okamura. 2009. Voltage-gated proton channel is expressed on phagosomes. *Biochem. Biophys. Res. Commun.* 382:274–279. http://dx.doi.org/10.1016/j.bbrc.2009.03.036

Payandeh, J., T. Scheuer, N. Zheng, and W.A. Catterall. 2011. The crystal structure of a voltage-gated sodium channel. *Nature.* 475:353–358. http://dx.doi.org/10.1038/nature10238

Perozo, E., D.M. Cortes, and L.G. Cuello. 1998. Three-dimensional architecture and gating mechanism of a K^+ channel studied by EPR spectroscopy. *Nat. Struct. Biol.* 5:459–469. http://dx.doi.org/10.1038/nsb0698-459

Perozo, E., D.M. Cortes, and L.G. Cuello. 1999. Structural rearrangements underlying K^+-channel activation gating. *Science.* 285:73–78. http://dx.doi.org/10.1126/science.285.5424.73

Qiu, F., S. Rebolledo, C. Gonzalez, and H.P. Larsson. 2013. Subunit interactions during cooperative opening of voltage-gated proton channels. *Neuron.* 77:288–298. http://dx.doi.org/10.1016/j.neuron.2012.12.021

Ramsey, I.S., M.M. Moran, J.A. Chong, and D.E. Clapham. 2006. A voltage-gated proton-selective channel lacking the pore domain. *Nature.* 440:1213–1216. http://dx.doi.org/10.1038/nature04700

Ramsey, I.S., E. Ruchti, J.S. Kaczmarek, and D.E. Clapham. 2009. Hv1 proton channels are required for high-level NADPH oxidase-dependent superoxide production during the phagocyte respiratory burst. *Proc. Natl. Acad. Sci. USA.* 106:7642–7647. http://dx.doi.org/10.1073/pnas.0902761106

Rees, D.C., L. DeAntonio, and D. Eisenberg. 1989. Hydrophobic organization of membrane proteins. *Science.* 245:510–513. http://dx.doi.org/10.1126/science.2667138

Sakata, S., T. Kurokawa, M.H. Nørholm, M. Takagi, Y. Okochi, G. von Heijne, and Y. Okamura. 2010. Functionality of the voltage-gated proton channel truncated in S4. *Proc. Natl. Acad. Sci. USA.* 107:2313–2318. http://dx.doi.org/10.1073/pnas.0911868107

Sasaki, M., M. Takagi, and Y. Okamura. 2006. A voltage sensor-domain protein is a voltage-gated proton channel. *Science.* 312:589–592. http://dx.doi.org/10.1126/science.1122352

Strelkov, S.V., and P. Burkhard. 2002. Analysis of α-helical coiled coils with the program TWISTER reveals a structural mechanism for stutter compensation. *J. Struct. Biol.* 137:54–64. http://dx.doi.org/10.1006/jsbi.2002.4454

Taylor, A.R., C. Brownlee, and G.L. Wheeler. 2012. Proton channels in algae: reasons to be excited. *Trends Plant Sci.* 17:675–684. http://dx.doi.org/10.1016/j.tplants.2012.06.009

Tombola, F., M.H. Ulbrich, and E.Y. Isacoff. 2008. The voltage-gated proton channel Hv1 has two pores, each controlled by one voltage sensor. *Neuron.* 58:546–556. http://dx.doi.org/10.1016/j.neuron.2008.03.026

Tombola, F., M.H. Ulbrich, S.C. Kohout, and E.Y. Isacoff. 2010. The opening of the two pores of the Hv1 voltage-gated proton channel is tuned by cooperativity. *Nat. Struct. Mol. Biol.* 17:44–50. http://dx.doi.org/10.1038/nsmb.1738

Villalba-Galea, C.A., W. Sandtner, D.M. Starace, and F. Bezanilla. 2008. S4-based voltage sensors have three major conformations. *Proc. Natl. Acad. Sci. USA.* 105:17600–17607. http://dx.doi.org/10.1073/pnas.0807387105

Wu, J., and H.R. Kaback. 1997. Helix proximity and ligand-induced conformational changes in the lactose permease of *Escherichia coli* determined by site-directed chemical crosslinking. *J. Mol. Biol.* 270:285–293. http://dx.doi.org/10.1006/jmbi.1997.1099

Wu, J., D. Hardy, and H.R. Kaback. 1998. Tilting of helix I and ligand-induced changes in the lactose permease determined by site-directed chemical cross-linking in situ. *Biochemistry.* 37:15785–15790. http://dx.doi.org/10.1021/bi981501o